IEEE Access
Multidisciplinary | Rapid Review | Open Access Journal

Received July 22, 2019, accepted August 4, 2019, date of publication August 7, 2019, date of current version September 3, 2019.

Digital Object Identifier 10.1109/ACCESS.2019.2933634

Study of the Terahertz Wave Scattering From Metal Surface Coated by Rough Lossy Coating Based on a Ray Tracing Modeling

RUI WANG, GUANGBIN GUO, AND LIXIN GUO, (Senior Member, IEEE)
School of Physics and Optoelectronic Engineering, Xidian University, Xi'an 710071, China

Corresponding author: Lixin Guo (lxguo@xidian.edu.cn)

This work was supported in part by the National Natural Science Foundation of Shaanxi Province under Grant 2018JQ6045, in part by the National Natural Science Foundation of China under Grant 61871457, Grant 61971338, and Grant 41806210, in part by the Foundation for Innovative Research Groups of the National Natural Science Foundation of China under Grant 61621005, and in part by the Shanghai Aerospace Science and Technology Innovation Foundation.

ABSTRACT A ray tracing method based on the geometrical optics and physical optics approximation is proposed for calculation of the scattering from rough metal surface with rough coating in terahertz regime. Geometrical optics is utilized to describe the wave propagation concerning the reflection and transmission, whereas physical optics is applied to obtain the scattering fields by equivalent currents on the surfaces. The method provides a reliable treatment of scattering from rough layers involving identical/different roughness. The scattering predictions of the rough layers are compared to the multilevel fast multipole algorithm (MLFMA) to demonstrate the efficiency and accuracy of the proposed method. Once validated, we use the method to carry out a sensitivity study of the bistatic radar scattering cross section to variations in layer parameters of interest in terahertz coating target detection, such as the roughness of the coating and metal surface, thickness of the coating layer.

INDEX TERMS Electromagnetic scattering, terahertz regime, ray tracing, rough coating.

I. INTRODUCTION

The investigation on the scattering characteristics of objects at the terahertz frequencies is very important because of the advantages of the terahertz wave for active detection, e.g., terahertz radar applications [1]. Reference [2] investigated the electromagnetic (EM) scattering characteristics of perfectly electrical conducting targets in the terahertz regime through the use of ray-based high-frequency techniques. Unfortunately, [2] suppose the surfaces of the objects are smooth. It is well-known that the terahertz wavelength is far smaller than that of millimeter and may be close to the roughness of the objects' surface. Hence, the reasonable assumptions that the surface of objects are smooth are inappropriate at terahertz frequencies. Some experiment have demonstrated the minor surface features can affect the terahertz scattering behavior of metallic objects [3], that is to say, the surface roughness can modulate more information of the object onto the scattering fields at terahertz frequencies and may bring crucial evidence for automatic object recognition in the terahertz radar applications although it produce big challenges to scattering computation. Therefore, it is necessary to study the EM scattering characteristics of object with rough surface at terahertz frequency. At present, some researchers have studied the scattering from objects considering the roughness in the terahertz frequencies and obtained theoretical and experimental achievements [1], [4], [5].

Due to various demands, the radar objects are usually coated with certain materials, such as radar absorbing materials. The scattering characteristics of the coated objects are significantly different from those of the uncoated objects. Presently, most of the studies concerning the EM scattering characteristics of coated objects mainly concentrate on microwave frequencies [6]-[8]. Hence, the surfaces of the object and coating mentioned in [6]–[8] are often supposed to be smooth. In reality, both the metal and coating surfaces should be considered as rough surfaces at the terahertz frequencies and the scattering from the rough case is more complex than that from the smooth case in the terahertz frequencies. Thus, there is few research focusing on the scattering characteristics of the rough case. This paper is focus on the sensitivity study of the terahertz wave scattering from

The associate editor coordinating the review of this article and approving it for publication was Lei Zhao.

rough metal surface with rough coating. The investigation in this paper is a foundation for studying the EM scattering behavior of the military targets coated by rough material in terahertz regime which is our planned work. The problem is related to the scattering of layered rough surfaces. An appropriate treatment of the layered rough surface is essential for sufficiently accurate EM field modeling in terahertz wave radiation and scattering problems.

At present, the scattering from rough surface has always been a typical and important problem in the field of EM scattering and remote sensing [9]. Many approaches have been proposed to study the scattering of the rough surface, including fully numerical methods and analytical methods. The fully numerical methods can give exact results while it will take more time when employing it to solve the scattering from multilayer rough interfaces. The empirical approach [10] based on the some experimental data can give accurate results, but cannot clarify the physical scattering mechanism. Some more efficient analytical techniques such as Kirchhoff approximation [11], multilayer stabilized extended boundary condition method (M-SEBCM) [12], and small perturbation method (SPM) [13]–[17] are proposed to deal with the scattering from a multilayered rough surface structure. Such studies have been studied on rough surface scattering subject, their focus are to get the scattering coefficient of the rough surface, which is a real number. Besides, the object of these research works is usually terrain and ocean surface based on certain PDF (probability density function) that can be simply tread as an infinite rough plate. The scattering data are used to determine the subsurface properties of natural layered rough surface structures [18] and the analytical results can be applied to the modeling of natural layered media such as ice and sand layers.

However, the target can no longer be regarded as an infinitely rough surface in the application of terahertz radar and the echo signals are complex number with phase information, which cannot be provided by the scattering theory of rough surface. To date, most researchers utilize high-frequency methods based on geometrical optics, physics optics, and shooting and bouncing ray (SBR) technique for the problems of terahertz scattering [19], [20]. However, these methods have been applied for smooth surfaces and few study have been done concerning the rough surface. We presented an approximate scattering modeling for simulation of the layered rough structure in terahertz regime based on physical optics method [21]. The model is valid for thin rough layered surface with low incident angles. The thickness and roughness of the coating are assumed to be small, besides that, the model suppose that two layered rough interfaces have same height PDF. In these cases, a good approximation of the reflection at this structure is to solve a single effective reflection coefficient at the coating interface. However, the roughness of layered surfaces is not always the same in reality. In other words, the profile of the coating rough surface is often different from that of the metal layer. Hence, there is still a great challenge presently in terahertz regime to simulate the scattering from the metal surface with coating materials having different roughness.

To solve this problem, the paper present a ray tracing method based on the geometrical optics and physical optics approximation for calculation of the scattering from finite rough metal surface with rough coating. Geometrical optics is utilized to describe the wave propagation concerning the reflection and transmission, whereas physical optics is applied to obtain the scattering fields by equivalent currents on the surfaces. Our method can provide both the average scattering coefficient and the complex scattering signals with phase information based for terahertz radar imaging. More important, the simulation model proposed in this paper can be extended the terahertz wave scattering modeling of the coated target in the future work. Validation of our model is performed by comparisons with MLFMA. Once validated, we use the method to carry out a sensitivity study of the bistatic scattering radar cross section (RCS) to variations in layer parameters of interest in terahertz coating target detection, such as the roughness of the coating and metal surface, thickness of the coating layer.

The paper is organized as follows. Section II describe the scattering strategy and theoretical formula of the method in details. Section III contains the model validation results against MLFMA. In Section IV, the sensitivity study of the scattering to variations in layer parameters of interest are shown. Section V ends with the conclusions of this paper and recommendations for further investigation.

II. THE SCATTERING STRATEGY AND THEORETICAL FORMULA

Fig. 1 visualizes ray propagation in dielectric coating layer on a rough underlying layer. As shown in Fig. 1, S_1 denotes the air-coating interface. (ε_1, μ_1) is the permittivity and permeability of the coating material and S_2 denotes the underlying layer surface. Plane triangle meshes are used for surface modeling. The incident wave $\boldsymbol{E}_i$ in Ω_0 arrive at the coating surface and induce the scattered fields $\boldsymbol{E}_{s1}$. The transmitted field $\boldsymbol{E}_1^T$ can be obtained based on Fresnel transmission coefficients. The incident field reaching the plane triangle mesh of the metal surface can be gotten from $\boldsymbol{E}_1^T$ by considering the attenuation of the wave in the coating material layer and the reflected field $\boldsymbol{E}_{12}^R$ on the same triangle mesh can be described

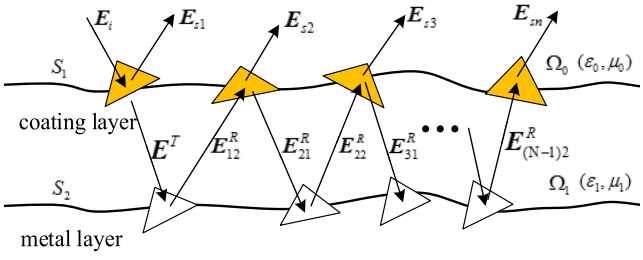

FIGURE 1. Ray tracing process of our method in the coating layer.

by using Fresnel reflection coefficients. Also, the incident field $\boldsymbol{E}_{12}^{i}$ reaching the metal surface of S_1 can be calculated from $\boldsymbol{E}_{12}^{R}$ by considering the attenuation of the wave in the coating material layer. Then $\boldsymbol{E}_{s2}$ can be obtained by means of the equivalent currents density on S_1 solved by $\boldsymbol{E}_{12}^{i}$ based on physical optical approximation. Keeping track of the rays and $\boldsymbol{E}_{sn}$ (n = 1, 2, 3 . . .) for every bounce can be gotten.

A. WAVE PROPAGATION THROUGH THE ROUGH LAYERED SURFACE

As shown in Fig. 2, consider the scattering configuration of the coated metal surface illuminated by an plane wave. Let $\boldsymbol{k}_i$ and $\boldsymbol{k}_s$ signify the incident and scattering vectors, respectively. θ_i and θ_s are the incident and scattered angles, while φ_i and φ_s are the incident and scattering azimuthal angles, respectively.

$$\begin{aligned}\hat{\boldsymbol{k}}_i &= -\sin\theta_i\cos\varphi_i\hat{\boldsymbol{x}} - \sin\theta_i\sin\varphi_i\hat{\boldsymbol{y}} - \cos\theta_i\hat{\boldsymbol{z}}\\ \hat{\boldsymbol{k}}_s &= \sin\theta_s\cos\varphi_s\hat{\boldsymbol{x}} + \sin\theta_s\sin\varphi_s\hat{\boldsymbol{y}} + \cos\theta_s\hat{\boldsymbol{z}}\end{aligned} \tag{1}$$

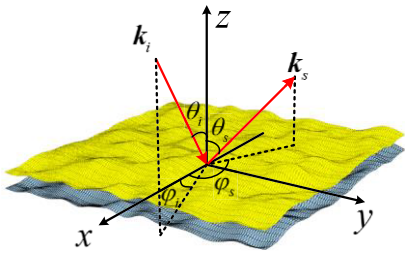

FIGURE 2. Geometry for scattering by a rough layer.

In the paper, the waves are assumed to exhibit a time-harmonic dependence according to $\exp(j\omega t)$, so that the propagation in space can be expressed by the factor $\exp(-j\boldsymbol{k}\cdot\boldsymbol{r})$. The incident field can be given by the following

$$\boldsymbol{E}_i(\boldsymbol{r}) = \boldsymbol{e}_i\exp(-j\boldsymbol{k}_i\cdot\boldsymbol{r}),\ \boldsymbol{H}_i(\boldsymbol{r}) = \boldsymbol{h}_i\exp(-j\boldsymbol{k}_i\cdot\boldsymbol{r}) \tag{2}$$

The main task of the approach is the computation of reflected and transmitted waves at the interfaces. As can be seen from Fig.1, there are mainly three general cases of the ray propagation in coating layer shown as in Fig.3-5.

Case 1: As shown in Fig.3, the scattered fields $\boldsymbol{E}_{s1}$ can be calculated from the equivalent EM currents based on the incident wave $\boldsymbol{E}_i$ reaching the coating surface.

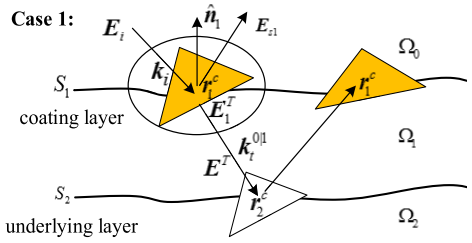

FIGURE 3. The first propagation case in the rough coating layer.

In this paper, a general formulation of transmission and reflection wave for a general interface between two different media is written as

$$\begin{aligned}\boldsymbol{E}(\boldsymbol{r}) &= \left\{\begin{array}{l}\zeta_{\mathrm{TE}}^{m|n}\left[\boldsymbol{E}^I(\boldsymbol{r}^c)\cdot\hat{\boldsymbol{e}}_{\mathrm{TE}}\right]\hat{\boldsymbol{e}}_{\mathrm{TE}}\\ +\zeta_{\mathrm{TM}}^{m|n}\left[\boldsymbol{E}^I(\boldsymbol{r}^c)\cdot\hat{\boldsymbol{e}}_{\mathrm{TM}}\right](\hat{\boldsymbol{e}}_{\mathrm{TE}}\times\hat{\boldsymbol{k}}_{\zeta}^{m|n})\end{array}\right\}e^{-j\boldsymbol{k}_{\zeta}^{m|n}\cdot(\boldsymbol{r}-\boldsymbol{r}^c)}\\ &= \boldsymbol{E}_a(\boldsymbol{r})e^{-j\boldsymbol{k}_{\zeta}^{m|n}\cdot(\boldsymbol{r}-\boldsymbol{r}^c)}\end{aligned} \tag{3}$$

$$\begin{aligned}\boldsymbol{H}(\boldsymbol{r}) &= \left\{\begin{array}{l}\zeta_{\mathrm{TE}}^{m|n}\left[\boldsymbol{H}^I(\boldsymbol{r}^c)\cdot(-\hat{\boldsymbol{e}}_{TM})\right]\left(\hat{\boldsymbol{k}}_{\zeta}^{m|n}\times\hat{\boldsymbol{e}}_{TE}\right)\\ +\zeta_{\mathrm{TM}}^{m|n}\left[\boldsymbol{H}^I(\boldsymbol{r}^c)\cdot\hat{\boldsymbol{e}}_{TE}\right]\hat{\boldsymbol{e}}_{TE}\end{array}\right\}e^{-j\boldsymbol{k}_{\zeta}^{m|n}\cdot(\boldsymbol{r}-\boldsymbol{r}^c)}\\ &= \boldsymbol{H}_a(\boldsymbol{r})e^{-j\boldsymbol{k}_{\zeta}^{m|n}\cdot(\boldsymbol{r}-\boldsymbol{r}^c)}\end{aligned} \tag{4}$$

here, $\zeta_{\mathrm{TE}}^{m|n}$ and $\zeta_{\mathrm{TM}}^{m|n}$ denote the Fresnel transmission or reflection coefficients, respectively. $\boldsymbol{k}_{\zeta}^{m|n}$ represents the reflected or transmitted wave vector. The superscript m and$n$ can be 0∼2, which represent $\Omega_0 \sim \Omega_2$. $\boldsymbol{r}^c$ is at the center of every subdivision surface element on the surface. Then, the transmission and reflection waves for different interfaces and incident directions can be obtained by simply setting parameters of media in general formula. Then the transmitted EM fields in Ω_1 can be written $\boldsymbol{E}^T(\boldsymbol{r})$ and $\boldsymbol{H}^T(\boldsymbol{r})$ from (3) and (4) by

$$\begin{aligned}&\boldsymbol{E}^I(\boldsymbol{r}^c)\to\boldsymbol{E}_i(\boldsymbol{r}_1^c),\quad \boldsymbol{H}^I(\boldsymbol{r}^c)\to\boldsymbol{H}_i(\boldsymbol{r}_1^c)\\ &\hat{\boldsymbol{k}}_{\zeta}^{m|n}\to\hat{\boldsymbol{k}}_t^{0|1},\quad \boldsymbol{k}_{\zeta}^{m|n}\to\boldsymbol{k}_t^{0|1},\ \zeta_{\mathrm{TE}}^{m|n}\to T_{TE}^{0|1},\ \zeta_{\mathrm{TM}}^{m|n}\to T_{TM}^{0|1}\end{aligned} \tag{5}$$

here, $\boldsymbol{r}_1^c$ is at the center of every subdivision surface element on the coating surface. $T_{TM}^{1|0}$ an $T_{TE}^{1|0}$ are the transmission coefficients of S_1^{low} (the lower surface of S_1) for TM and TE waves, respectively. $\hat{\boldsymbol{e}}_{TE}$ and $\hat{\boldsymbol{e}}_{TM}$ are the normalized direction of TE and TM waves, respectively

$$\hat{\boldsymbol{e}}_{TE} = \frac{\hat{\boldsymbol{k}}_I\times\hat{\boldsymbol{n}}}{\left|\hat{\boldsymbol{k}}_I\times\hat{\boldsymbol{n}}\right|},\quad \hat{\boldsymbol{e}}_{TM} = \hat{\boldsymbol{e}}_{TE}\times\hat{\boldsymbol{k}}_I \tag{6}$$

here $\hat{\boldsymbol{k}}_I = \hat{\boldsymbol{k}}_i, \hat{\boldsymbol{n}} = \hat{\boldsymbol{n}}_1, \hat{\boldsymbol{n}}_1$is the normal unit vector of S_1^{upp}.

As a consequence of the boundary conditions, the tangential components of all wave vectors are continuous. Thus, the transmission wave vector $\boldsymbol{k}_t^{0|1}$ can be obtained by the following

$$\boldsymbol{k} = k_t\hat{\boldsymbol{t}} + k_n\hat{\boldsymbol{n}} \tag{7}$$

In order to implement the ray-tracing process, it is also necessary to obtain the propagation direction of the transmitted wave. For a lossy medium, the transmitted wave is nonuniform. The directions of constant phase and amplitude planes of the nonuniform wave are not identical. So, in the most general case, the propagation direction of transmitted wave $\hat{\boldsymbol{k}}_t^{0|1}$ can be given by the following

$$\hat{\boldsymbol{k}} = \frac{\mathrm{Real}(k_t)\hat{\boldsymbol{t}} + \mathrm{Real}(k_n)\hat{\boldsymbol{n}}}{\left|\mathrm{Real}(k_t)\hat{\boldsymbol{t}} + \mathrm{Real}(k_n)\hat{\boldsymbol{n}}\right|} \tag{8}$$

here, Real(·) denotes the real part. In order to solve $\boldsymbol{k}_t^{0|1}$ and $\hat{\boldsymbol{k}}_t^{0|1}$, $k_t = k_{1t} = \boldsymbol{k}_i\cdot\hat{\boldsymbol{t}}_1, k_n = k_{1n} = -\sqrt{k_1^2 - k_{1t}^2}$,

$\hat{\boldsymbol{t}} = \hat{\boldsymbol{t}}_1, \hat{\boldsymbol{n}} = \hat{\boldsymbol{n}}_1$ in (7) and (8). k_1 is characterized by the dispersion relations

$$k_1^2 = \omega^2 \varepsilon_1 \mu_1 \tag{9}$$

$\hat{\boldsymbol{t}}_1$ denotes the tangential unit vector of the triangle mesh of S_1^{upp} and can be obtained as

$$\hat{\boldsymbol{t}}_1 = \hat{\boldsymbol{n}}_1 \times (\hat{\boldsymbol{k}}_i \times \hat{\boldsymbol{n}}_1) \tag{10}$$

Case 2: Fig. 4 shows the reflected scattering of the metal surface. The transmission wave reaching the center of every subdivision surface element $\boldsymbol{r}_2^c$ on S_2 in Fig. 4 should be described as $\boldsymbol{E}^T(\boldsymbol{r}_2^c)$ and $\boldsymbol{H}^T(\boldsymbol{r}_2^c)$ based on (5).

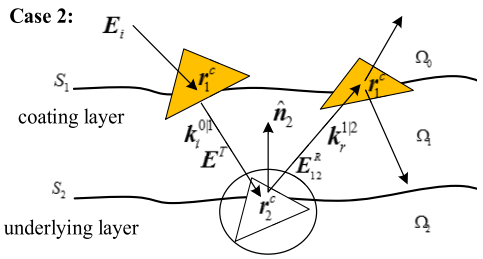

FIGURE 4. The second propagation case in the rough coating layer.

Then with the aid of Fresnel law of reflection, the reflected EM fields $\boldsymbol{E}_{12}^R(\boldsymbol{r})$ and $\boldsymbol{H}_{12}^R(\boldsymbol{r})$ of metal surface can be gotten from (3) and (4) by

$$\begin{aligned} &\boldsymbol{E}^I(\boldsymbol{r}^c) \to \boldsymbol{E}^T(\boldsymbol{r}_2^c),\ \boldsymbol{H}^I(\boldsymbol{r}^c) \to \boldsymbol{H}^T(\boldsymbol{r}_2^c) \\ &\hat{\boldsymbol{k}}_\zeta^{m|n} \to \hat{\boldsymbol{k}}_r^{1|2},\quad \boldsymbol{k}_\zeta^{m|n} \to \boldsymbol{k}_r^{1|2},\ \zeta_{\text{TE}}^{m|n} \to R_{TE}^{1|2},\ \zeta_{\text{TM}}^{m|n} \to R_{TM}^{1|2} \end{aligned} \tag{11}$$

here, $R_{TE}^{1|2}$ and $R_{TM}^{1|2}$ are the Fresnel reflection coefficients of upper surface of S_2 (S_2^{upp}) for TM and TE waves, respectively. $\hat{\boldsymbol{e}}_{TE}$ and $\hat{\boldsymbol{e}}_{TM}$ can be obtained by (6) with $\hat{\boldsymbol{k}}_I = \hat{\boldsymbol{k}}_t^{0|1}, \hat{\boldsymbol{n}} = \hat{\boldsymbol{n}}_2$. $\hat{\boldsymbol{n}}_2$ is the normal unit vector of S_2^{upp} (Fig. 4). Similar to case 1, $\boldsymbol{k}_r^{1|2}$ and $\hat{\boldsymbol{k}}_r^{1|2}$ can be solved by (7) and (8) with $k_t = k'_{1t} = \boldsymbol{k}_t^{0|1} \cdot \hat{\boldsymbol{t}}_2, k_n = k'_{1n} = \sqrt{k_1^2 - k'^2_{1t}}, \hat{\boldsymbol{t}} = \hat{\boldsymbol{t}}_2, \hat{\boldsymbol{n}} = \hat{\boldsymbol{n}}_2$. $\hat{\boldsymbol{t}}_2$ is the tangential unit vector of the triangle mesh of S_2^{upp} and can be obtained as

$$\hat{\boldsymbol{t}}_2 = \hat{\boldsymbol{n}}_2 \times (\hat{\boldsymbol{k}}_t^{0|1} \times \hat{\boldsymbol{n}}_2) \tag{12}$$

Case 3: Fig. 5 shows the transmission and reflected scattering of the coating surface, respectively. The incident wave reaching the air-coating interface shown as in Fig. 5 should be described as $\boldsymbol{E}_{12}^R(\boldsymbol{r}_1)$ and $\boldsymbol{H}_{12}^R(\boldsymbol{r}_1)$ based on (11).

By using Fresnel law of transmission, the transmitted fields through the coating surface can be written as $\boldsymbol{E}_{21}^T(\boldsymbol{r}_1)$ and $\boldsymbol{H}_{21}^T(\boldsymbol{r}_1)$. They can be solved from $\boldsymbol{E}_a(\boldsymbol{r})$ and $\boldsymbol{H}_a(\boldsymbol{r})$ in (3) and (4) by

$$\begin{aligned} &\boldsymbol{E}^I(\boldsymbol{r}^c) \to \boldsymbol{E}_{12}^R(\boldsymbol{r}_1),\quad \boldsymbol{H}^I(\boldsymbol{r}^c) \to \boldsymbol{H}_{12}^R(\boldsymbol{r}_1) \\ &\hat{\boldsymbol{k}}_\zeta^{m|n} \to \hat{\boldsymbol{k}}_t^{1|0},\quad \boldsymbol{k}_\zeta^{m|n} \to \boldsymbol{k}_t^{1|0},\ \zeta_{\text{TE}}^{m|n} \to T_{TE}^{1|0},\ \zeta_{\text{TM}}^{m|n} \to T_{TM}^{1|0} \end{aligned} \tag{13}$$

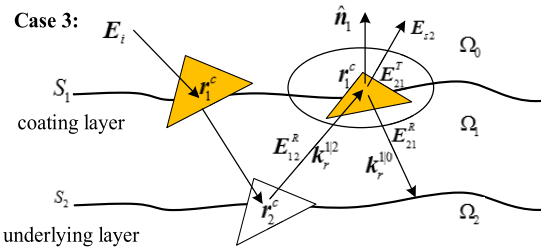

FIGURE 5. The third propagation case in the rough coating layer.

here, $T_{TM}^{1|0}$ an $T_{TE}^{1|0}$ are the transmission coefficients of S_1^{low} (the lower surface of S_1) for TM and TE waves, respectively. $\hat{\boldsymbol{e}}_{TE}$ and $\hat{\boldsymbol{e}}_{TM}$ can be obtained by (6) with $\hat{\boldsymbol{k}}_I = \hat{\boldsymbol{k}}_r^{1|2}, \hat{\boldsymbol{n}} = \hat{\boldsymbol{n}}_1$. Similar to case 1, $\boldsymbol{k}_t^{1|0}$ and $\hat{\boldsymbol{k}}_t^{1|0}$ can be solved by (7) and (8) with $k_t = k_{0t} = \boldsymbol{k}_r^{1|2} \cdot \hat{\boldsymbol{t}}_1, k_n = k_{0n} = \sqrt{k_0^2 - k_{0t}^2}, \hat{\boldsymbol{t}} = \hat{\boldsymbol{t}}_1, \hat{\boldsymbol{n}} = \hat{\boldsymbol{n}}_1$. k_0 is characterized by the dispersion relations

$$k_0^2 = \omega^2 \varepsilon_0 \mu_0 \tag{14}$$

Then the surface equivalent currents density on the coating surface can be solved based on physical optical approximation to obtain $\boldsymbol{E}_{s2}$ considering one reflection at S_2 (See subsection *B* of section II for details).

In order to solve the scattered fields $\boldsymbol{E}_{sn}$, it needs to keep track of the rays. The reflected wave on S_1 into Ω_1 can be written as $\boldsymbol{E}_{21}^R(\boldsymbol{r}), \boldsymbol{H}_{21}^R(\boldsymbol{r})$. They can be solved from (3) and (4) by

$$\begin{aligned} &\boldsymbol{E}^I(\boldsymbol{r}^c) \to \boldsymbol{E}_{12}^R(\boldsymbol{r}_1^c),\quad \boldsymbol{H}^I(\boldsymbol{r}^c) \to \boldsymbol{H}_{12}^R(\boldsymbol{r}_1^c) \\ &\hat{\boldsymbol{k}}_\zeta^{m|n} \to \hat{\boldsymbol{k}}_r^{1|0},\quad \boldsymbol{k}_\zeta^{m|n} \to \boldsymbol{k}_r^{1|0},\ \zeta_{\text{TE}}^{m|n} \to R_{TE}^{1|0},\ \zeta_{\text{TM}}^{m|n} \to R_{TM}^{1|0} \end{aligned} \tag{15}$$

here, $R_{TE}^{1|0}$ and $R_{TM}^{1|0}$ are the Fresnel reflection coefficients of S_1^{low} for TM and TE waves, respectively. $\hat{\boldsymbol{e}}_{TE}$ and $\hat{\boldsymbol{e}}_{TM}$ can be obtained by (6) with $\hat{\boldsymbol{k}}_I = \hat{\boldsymbol{k}}_r^{1|2}, \hat{\boldsymbol{n}} = \hat{\boldsymbol{n}}_1$. Similar to Case 1, $\boldsymbol{k}_r^{1|0}$ and $\hat{\boldsymbol{k}}_r^{1|0}$ can be solved by (7) and (8) with $k_t = k''_{1t} = \boldsymbol{k}_r^{1|2} \cdot \hat{\boldsymbol{t}}_1, k_n = k''_{1n} = -\sqrt{k_1^2 - k''^2_{1t}}, \hat{\boldsymbol{t}} = \hat{\boldsymbol{t}}_1, \hat{\boldsymbol{n}} = \hat{\boldsymbol{n}}_1$.

Then the incident EM fields reaching S_2^{upp} can be obtained from $\boldsymbol{E}_{21}^R(\boldsymbol{r}_2^c)$ and $\boldsymbol{H}_{21}^R(\boldsymbol{r}_2^c)$. Case 2 and case 3 are carried out alternately and repeatedly in following ray tracing process.

B. THE COMPUTIONS OF THE SCATTERED FIELDS

By using physic optical approximation, the EM far fields can be expressed in terms of the equivalent EM currents based on Stratton-Chu formula [23] as

$$\begin{aligned} \boldsymbol{E}_s = jk_0 \frac{e^{-jkr}}{4\pi r} \int_s \hat{\boldsymbol{k}}_s \times \left[\hat{\boldsymbol{k}}_s \times \sqrt{\frac{\mu_0}{\varepsilon_0}} \boldsymbol{J}(\boldsymbol{r}_1') + \boldsymbol{M}(\boldsymbol{r}_1') \right] \\ \times e^{j\boldsymbol{k}_s \cdot \boldsymbol{r}_1'} \mathrm{d}S' \end{aligned} \tag{16}$$

$$\begin{aligned} \boldsymbol{H}_s = -jk_0 \frac{e^{-jkr}}{4\pi r} \int_s \hat{\boldsymbol{k}}_s \times \left[\boldsymbol{J}(\boldsymbol{r}_1') - \sqrt{\frac{\varepsilon_0}{\mu_0}} \hat{\boldsymbol{k}}_s \times \boldsymbol{M}(\boldsymbol{r}_1') \right] \\ \times e^{j\boldsymbol{k}_s \cdot \boldsymbol{r}_1'} \mathrm{d}S' \end{aligned} \tag{17}$$

where, the observation point $\boldsymbol{r}$ is in Ω_0. $\boldsymbol{r}'$ denotes the source point on S_1^{upp}. It should be noted that (18) and (19) are derived by means of the far-field approximation that observation point $\boldsymbol{r}$ is very far away from source point $\boldsymbol{r}'$. The equivalent EM currents based on physic optical can be written as

$$\boldsymbol{J}_n = \begin{cases} \hat{\boldsymbol{n}}_1 \times \boldsymbol{H}_1^T = \hat{\boldsymbol{n}}_1 \times \boldsymbol{h}_1^T e^{-j\boldsymbol{k}_i \cdot \boldsymbol{r}_1'} = \boldsymbol{J}_{a1} e^{-j\boldsymbol{k}_i \cdot \boldsymbol{r}_1'} \\ \quad n = 1 \text{ (for Case 1)} \\ \hat{\boldsymbol{n}}_1 \times \boldsymbol{H}_{21}^T = \hat{\boldsymbol{n}}_1 \times \boldsymbol{h}_{21}^T e^{-j\boldsymbol{k}_i \cdot \boldsymbol{r}_1'} = \boldsymbol{J}_{an} e^{-j\boldsymbol{k}_r^{1|2} \cdot \boldsymbol{r}_1'} \\ \quad n \geq 2 \text{ (for Case 3)} \end{cases} \tag{18}$$

$$\boldsymbol{M}_n = \begin{cases} \boldsymbol{E}_1^T \times \hat{\boldsymbol{n}}_1 = \boldsymbol{e}_1^T \times \hat{\boldsymbol{n}}_1 e^{-j\boldsymbol{k}_i \cdot \boldsymbol{r}_1'} = \boldsymbol{M}_{a1} e^{-j\boldsymbol{k}_i \cdot \boldsymbol{r}_1'} \\ \quad n = 1 \text{ (for Case 1)} \\ \boldsymbol{E}_{21}^T \times \hat{\boldsymbol{n}}_1 = \boldsymbol{e}_{21}^T \times \hat{\boldsymbol{n}}_1 e^{-j\boldsymbol{k}_i \cdot \boldsymbol{r}_1'} = \boldsymbol{M}_{an} e^{-j\boldsymbol{k}_r^{1|2} \cdot \boldsymbol{r}_1'} \\ \quad n \geq 2 \text{ (for Case 3)} \end{cases} \tag{19}$$

By substituting (18)-(19) into (16)-(17), the scattered fields of subdivision surface can be respectively expressed as follows

$$\boldsymbol{E}_{sn} = jk_0 \frac{e^{-jkr}}{4\pi r} \hat{\boldsymbol{k}}_s \times \left[\hat{\boldsymbol{k}}_s \times \sqrt{\frac{\mu_0}{\varepsilon_0}} \boldsymbol{J}_{an} + \boldsymbol{M}_{an} \right] \times \int_s e^{-j(\boldsymbol{k}_I - \boldsymbol{k}_s) \cdot \boldsymbol{r}'} \mathrm{d}S' \tag{20}$$

$$\boldsymbol{H}_{sn} = jk_0 \frac{e^{-jkr}}{4\pi r} \hat{\boldsymbol{k}}_s \times \left[\sqrt{\frac{\varepsilon_0}{\mu_0}} \hat{\boldsymbol{k}}_s \times \boldsymbol{M}_{an} - \boldsymbol{J}_{an} \right] \times \int_s e^{-j(\boldsymbol{k}_I - \boldsymbol{k}_s) \cdot \boldsymbol{r}'} \mathrm{d}S' \tag{21}$$

here $n = 1, 2, 3 \cdots N$. N is the total number of the ray tracing. The surface integral part in (20)-(21) can be simplified as follows [22]

$$W = \int e^{-j(\boldsymbol{k}_I - \boldsymbol{k}_s) \cdot \boldsymbol{r}'} dS' = \int e^{-j\boldsymbol{\omega} \cdot \boldsymbol{r}'} dS' = \begin{cases} e^{-j\boldsymbol{\omega} \cdot \boldsymbol{r}_c'} \Delta S & \boldsymbol{\beta} = 0 \\ \dfrac{1}{j\boldsymbol{\beta}^2} \displaystyle\sum_{i=0}^{3} \left\{ \begin{array}{l} (\boldsymbol{\omega} \times \hat{\boldsymbol{n}}) \cdot (\boldsymbol{v}_{i+1} - \boldsymbol{v}_i) \\ \cdot e^{-j\boldsymbol{\omega} \cdot \frac{\boldsymbol{v}_i + \boldsymbol{v}_{i+1}}{2}} \sin c \left(\boldsymbol{\omega} \frac{\boldsymbol{v}_{i+1} - \boldsymbol{v}_i}{2} \right) \end{array} \right\} & \boldsymbol{\beta} \neq 0 \end{cases} \tag{22}$$

here $\boldsymbol{\omega} = \boldsymbol{k}_I - \boldsymbol{k}_s$. $\boldsymbol{k}_I$ denotes $\boldsymbol{k}_i$ for $\boldsymbol{E}_{s1}$ and $\boldsymbol{k}_r^{1|2}$ for $\boldsymbol{E}_{s2}$, respectively. $\boldsymbol{\beta} = \boldsymbol{\omega} - (\boldsymbol{\omega} \cdot \hat{\boldsymbol{n}}) \hat{\boldsymbol{n}}$ is the projection of vector $\boldsymbol{\omega}$ on the triangle mesh and $\boldsymbol{v}_i$ is the position vector of the ith vertex of the triangle mesh in the global coordinate. Substituting (22) into (20)-(21), the total fields from every mesh on S_1 can be expressed as follows

$$\boldsymbol{E}_{total}^s(\boldsymbol{r}) = \sum_{n=1}^{N} \boldsymbol{E}_{sn}(\boldsymbol{r}) \tag{23}$$

$$\boldsymbol{H}_{total}^s(\boldsymbol{r}) = \sum_{n=1}^{N} \boldsymbol{H}_{sn}(\boldsymbol{r}) \tag{24}$$

Then the total scattering fields is the superposition of scattering fields from all surface meshes on S_1.

III. VALIDATION OF THE SCATTERIGN MODEL

For excitation, a plane wave with $f = 1$THz is utilized. In all the following simulation examples, both the incident and scattering plane are the *xoz* plane (both $\boldsymbol{k}_i$ and $\boldsymbol{k}_s$ are set in *xoz* plane) and the receiving polarization mode is horizontal polarization.

A. THE SCATTERIGN FOR DIFFERENT BOUNCES

The bistatic RCS by our method under different bounces are presented in Fig. 6 and 7. The black solid RCS lines (no bounce) only consider the reflection of the incident plane wave at S_1. The colored lines represent the scattering from the rough layers where the wave undergoes one or more reflections at S_2 (corresponding to different bounces). Large errors are introduced by the black solid lines in Fig. 6 and 7 compared with the simulations considering ray propagation in the dielectric coating. The reason is that the simulation of the black solid lines doesn't take ray propagation in the dielectric coating into account (no reflection at S_2). Moreover, the incident wave can easily penetrate the air-coating interface because the relative permittivity of coating $\varepsilon_{r1} = 2.05 - j0.1$ is very close to that of air. Thus, the simulation of the black solid line is unreliable.

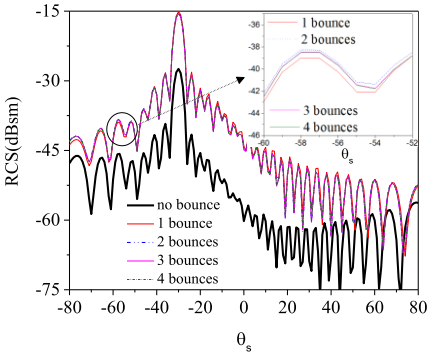

FIGURE 6. Bistatic RCS for a rough layer with identical roughness.

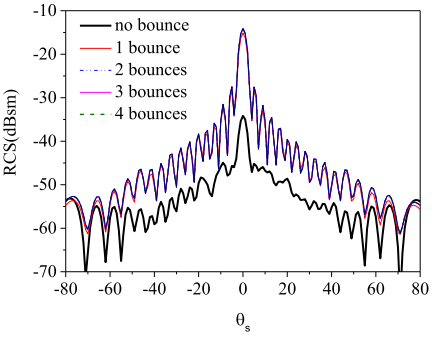

FIGURE 7. Bistatic RCS for a rough layer with different roughness.

It can be found that the simulations tend to be constant gradually with the increasing of the ray bounces in Fig.6. Moreover, there is no difference between the simulations based on three and four bounces. The conclusion from Fig. 6 are same as that from Fig. 7. The finding indicates

that the simulation considering three bounces corresponding to the maximum number of computed equivalent current contributions is sufficient to quantify the scattering process. Thus, three bounces are allowed in the dielectric coating for following simulations.

Since there is no relevant experimental measurement data at present, we evaluate the accuracy of our method by using classical numerical methods in section *B* and *C*.

B. THE TWO ROUGH SURFACE WITH IDENTICAL ROUGHNESS

As the degenerate cases, Fig. 8 compares the bistatic RCS of the smooth layers with dimensions $\Delta x \times \Delta y = 16\lambda \times 16\lambda$ by using our method with that by using MLFMA. It can be seen that RCS result of the smooth layers by our method is in a good agreement with that by MLFMA. When RCSs are relatively very small (smaller than -55 dB), there is the discrepancy between the RCSs curves. It is mainly due to that edge diffraction ignored in our method has a great influence on scattering for smooth case.

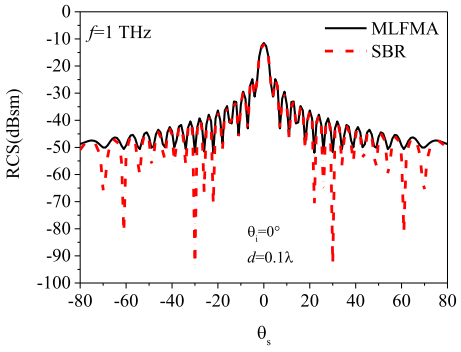

FIGURE 8. Bistatic RCS for a smooth layer.

For the rough case, we chose 10 realizations for the rough layer in the following results. Fig. 9 and 10 compare the bistatic RCS of the rough layers with identical profile by using our method with that by using MLFMA. The related parameters of two rough interfaces are presented in figures. The thickness of the coating layer in Fig.9 and 11 is 0.1λ and 0.3λ, respectively. δ and l are the root-mean-square (RMS) height and correlation length, respectively. d is the mean thickness of the coating layer. As can be seen in Fig. 9 and 10, a very good scattered field prediction near the specular direction is possible. The mean errors and computation time of our method are compared with that of MLFMA in Table. 1. As shown in the table, both the mean errors and the pear errors of the simulations by using two methods are acceptable. The ratio of the computation time approximates 1:46 and 1:60 for Fig. 9 and 10, respectively.

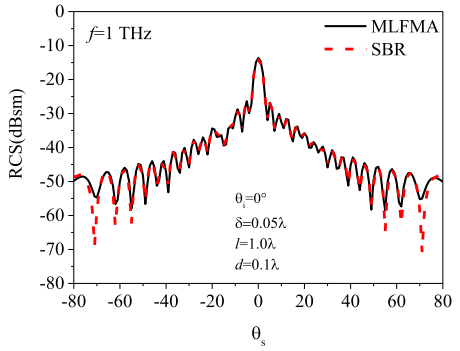

FIGURE 9. Bistatic RCS for a rough layer with identical roughness.

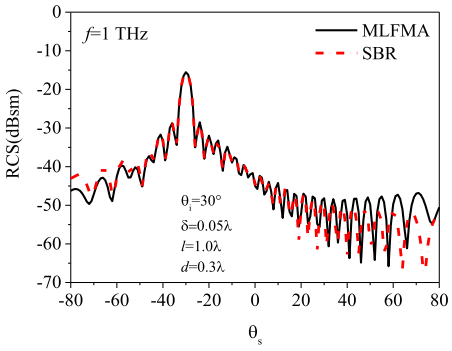

FIGURE 10. Bistatic RCS (hh) for a rough layer with identical roughness.

TABLE 1. Computation error and time for simulations.

	computation error (dB)		computation time (s)	
	Mean error	Peak error	Our method	MLFMA
Fig.9	0.9	0.07	500	22550
Fig.10	2.6	0.1	501	29930

C. THE ROUGH SURFACE WITH DIFFERENT ROUGHNESS

Fig.11-12 compares the bistatic RCS of the rough layers with different roughness by using our method with that by using MLFMA.

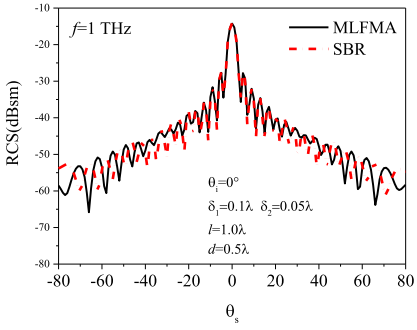

FIGURE 11. Bistatic RCS (hh) for a rough layer with different δ.

The related parameters of two rough interfaces are presented in figures. The similar conclusions can be found from these two figures. The mean errors and computation time of our method are compared with that of MLFMA in Table. 2. The ratio of the computation time approximates 1:54 and 1:56 for Fig. 11 and 12, respectively.

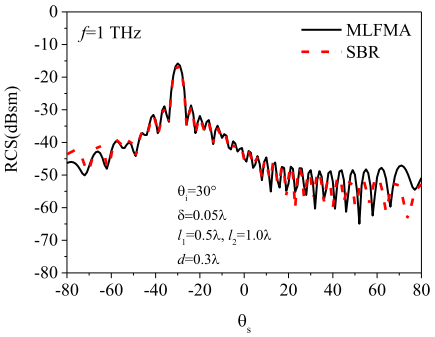

FIGURE 12. Bistatic RCS (hh) for a rough layer with different *l*.

TABLE 2. Computation error and time for simulations.

	computation error (dB)		computation time (s)	
	Mean error	Peak error	Our method	MLFMA
Fig.11	3.18	0.14	545	29960
Fig.12	2.25	0.30	539	30561

IV. NUMERICAL SIMULATIONS

The scattering from the coated metal surface is compared with that from uncoated metal surface in Fig. 13. The coating material is fiber reinforced plastic (FRP) with $\varepsilon_{r1} = 4.56 - j0.608$. The correlation length of the rough surface is 200 μm and the average thickness of the coating is 140 μm. The coating and metal surfaces have different RMS heights.

It can be found that, as the metal surface is coated by FRP, the RCS for most scattering angles decrease because the coated material is lossy. When the roughness of the metal layer is much larger than that of the coating layer, there is an interesting case shown in Fig. 13(d) that the RCS of the coated case is greater than the uncoated case (black solid line) for the specular scattering angles.

The phenomenon can be explained by comparing Fig. 13 (b) with Fig. 13 (d). The roughness of the metal layer in Fig. 13 (b) is as same as that in Fig. 13 (d), while the roughness of the coating layer in Fig. 13 (b) is larger than that in Fig.13 (d). We focus on the RCS for the specular scattering angles (S-RCS). When the metal layer is very rough, the wave reflected by the metal layer and then transmitted through the coating layer become weaker in the specular scattering direction. Hence, the S-RCS for coated case is greatly affected by the roughness of coating layer. When the coating layer is rough (Fig. 13 (b)), the S-RCS for the coated case is lower than that for the uncoated case. As the roughness of the coating decrease, the S-RCS for the coated case increase and even exceed the S-RCS for uncoated case (Fig. 13 (d)).

Next, fixing RMS height of coating surface (δ_1) to be 5 μm, changing the RMS height of metal surface (δ_2), the effect of roughness on bistatic RCS is studied in Fig. 14 for $f = 2$ Thz and $f = 6$ Thz, respectively. The coating material is poly tetra fluoroethylene (PTFE). Please be noted that the overall scattering can be very sensitive to the roughness of the metal. As the metal roughness increases, the incoherent

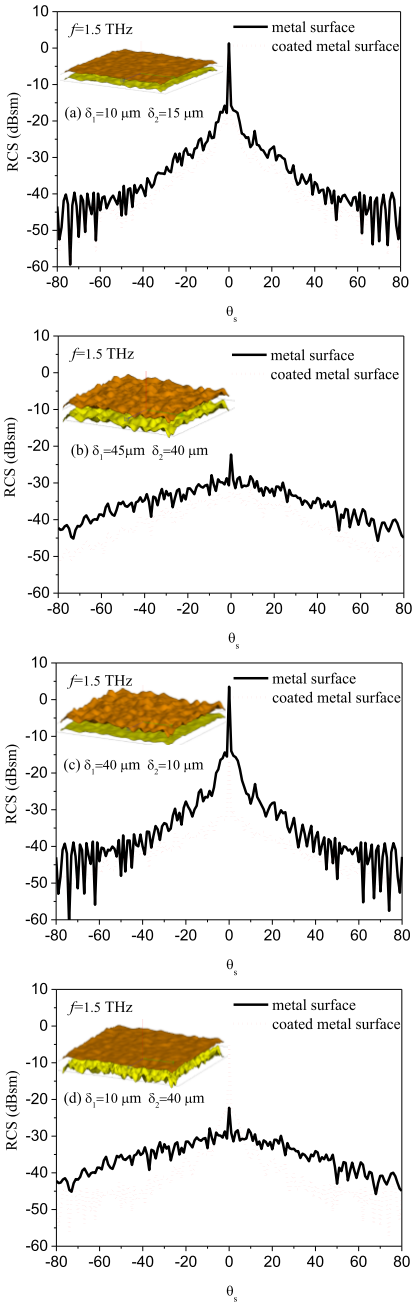

FIGURE 13. Comparison of the Bistatic RCS for coated metal surface with that for metal surface without coating.

scattering increases and the coherent scattering weakens. Keeping δ_2 constant, the bistatic RCS with increasing δ_1 are done in Fig. 15. It can be found that the RCS with different δ_1 appear similar. Their sensitivity to the RMS height of coating change is small. The main reason is the wave transmitted into coating easily with the dielectric parameters closed to that of the air. Hence, the variations in the coating roughness have very small effects on the results in most angles.

Finally, to see the effect of the thickness (d) of the coating, it is changed from tens to hundreds of microns. The results are depicted in Fig. 16 and Fig.18 for the coating being FRP and

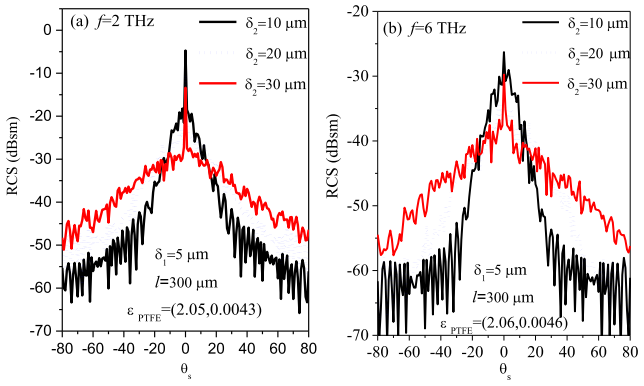

FIGURE 14. Bistatic RCS of coated metal surface versus the roughness of metal layer.

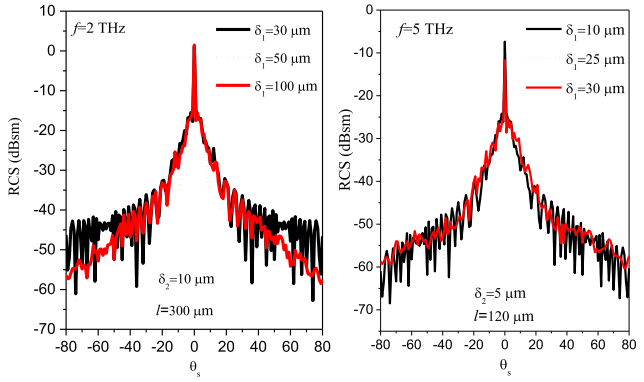

FIGURE 15. Bistatic RCS of coated metal surface versus the roughness of coating layer.

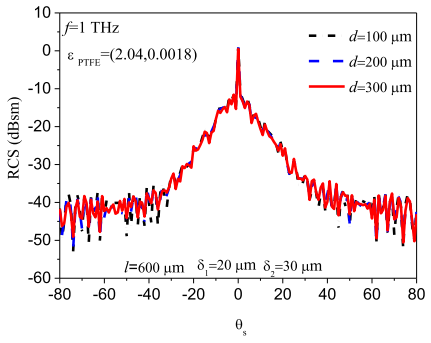

FIGURE 16. Bistatic RCS versus the thickness for PTFE coating.

PTFE, respectively. In Fig. 16, as the thickness increases from 50 μm to 300 μm, there is little difference can be observed, whereas in Fig. 18, this difference is obvious with the change of the thickness of the coating. This is consistent with the expectation that since the increased imaginary part of ε_{r1} raises the coating layer loss, the scattered fields are more sensitive to changes of d.

It should be noted that the RCS is not monotonic with respect to d for the coating being FRP as shown in Fig. 17. This is obvious since, by changing d of the coating layer in a certain range, the wave interference will be enhance or

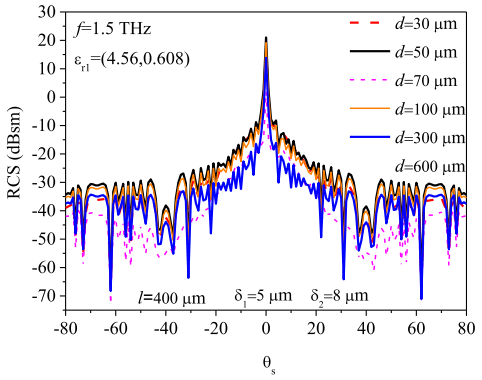

FIGURE 17. Bistatic RCS versus the thickness for FRP coating.

weakened. It is seen that, for larger d, the results tend to a certain limit which is associated with the layered structure.

Indeed, in accordance with [23], when d is larger than the wave penetration depth, the metal is not sensed by the waves and hence has no effect on the simulation. For lossy media, $\varepsilon_1 = \varepsilon_{r1}\varepsilon_0 = \varepsilon' - j\varepsilon''$ is complex. The wavenumber $\boldsymbol{k}$ is complex too. A wave propagating in a certain direction also decays exponentially in that direction. Let $\boldsymbol{k} = \boldsymbol{k}_R - j\boldsymbol{k}_I$, then the transmitted wave can be written as

$$\boldsymbol{E}_T = \boldsymbol{e}_t \exp\left[-(\boldsymbol{k}_I \cdot \boldsymbol{r})\right] \exp\left[-j\boldsymbol{k}_R \cdot \boldsymbol{r}\right] \tag{25}$$

Here, $\exp\left[-(\boldsymbol{k}_I \cdot \boldsymbol{r})\right]$ denotes wave amplitude attenuation and

$$\boldsymbol{k}_I = \left(\frac{\omega^2\mu\varepsilon'}{2}\left[\sqrt{1+\left(\frac{\varepsilon''}{\varepsilon'}\right)^2} - 1\right]\right)^{0.5} \tag{26}$$

Suppose the wave vertically incident upon the layer, (25)can be rewritten as

$$\boldsymbol{E}_T = \boldsymbol{e}_t \exp\left[-(k_I z)\right] \exp\left[-jk_R z\right] \tag{27}$$

here $z = 2d$.

Then we can give the variation of the wave amplitude attenuation coefficient (WAAC) with the thickness of the coating layer for the vertically incident case in Fig. 18. At $f = 1.5$ THz, for the chosen values of permittivity, the wave penetration depth is about 300 μm (since WAAC is

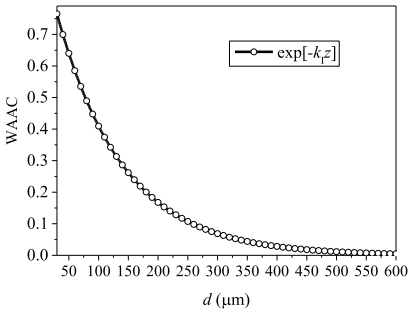

FIGURE 18. Wave amplitude attenuation coefficient versus d for FRP coating.

about 0.06), meaning that, in both the 300 μm∼600 μm separation cases, the metal is barely detected, and therefore their RCS appear similar (shown in Fig. 19). As expected, the RCS shown is not sensitive to change of the larger thickness and coincides with that of the coating layer only.

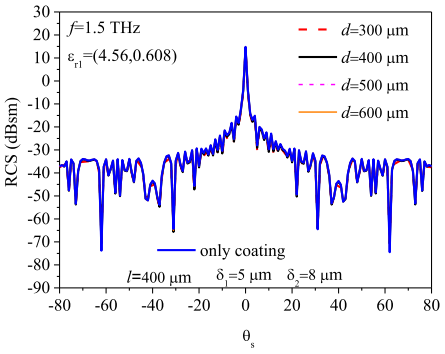

FIGURE 19. Bistatic RCS versus the thickness for FRP coating.

It should be noted that the RCS results in Fig. 17 and 19 are symmetrical about the direction of zero degree. This is mainly because that the roughness of the coating and metal surfaces in Fig. 17 and 19 are small, thus the RCS feature is close to that for smooth surface case.

V. CONCLUSION

A solution to EM scattering from rough metal with arbitrary dielectric coating for terahertz frequencies developed and presented in this work using a ray tracing method. The method can simulate the scattering from the rough layered structures with different roughness, which cannot be solved by using the approximate method proposed in Ref [21]. Our method can provide both the average scattering coefficient and the complex scattering signals with phase information based for terahertz radar imaging. More important, the simulation model proposed in this paper can be extended the terahertz wave scattering modeling of the coated target in the next work which cannot be provided by recent rough-surface scattering theories. Validation of our simulation model is performed by comparisons with MLFMA to demonstrate the efficiency and accuracy. A sensitivity study of the bistatic RCS to variations in layer parameters of interest in terahertz coating target detection, such as the roughness of the coating and metal surface, thickness of the coating layer is carry out by using our method.

The ray tracing model developed here is planned to be used in EM scattering and imaging of terahertz coated targets.

REFERENCES

[1] J. Gao, R. Wang, B. Deng, Y. Qin, H. Wang, and X. Li, "Electromagnetic scattering characteristics of rough PEC targets in the terahertz regime," *IEEE Antennas Wireless Propag. Lett.*, vol. 16, pp. 975–978, 2017.

[2] Z. Li, T. J. Cui, X. J. Zhong, Y. B. Tao, and H. Lin, "Electromagnetic scattering characteristics of PEC targets in the terahertz regime," *IEEE Antennas Propag. Mag.*, vol. 51, no. 1, pp. 39–50, Feb. 2009.

[3] A. Jagannathan, A. J. Gatesman, T. Horgan, T. Goyette, M. Coulombe, R. H. Giles, and W. E. Nixon, "Effect of periodic roughness and surface defects on the terahertz scattering behavior of cylindrical objects," *Proc. SPIE*, vol. 7671, Apr. 2010, Art. no. 76710E.

[4] M. Sun, Z. Cong, D. Ding, and R. Chen, "Terahertz scattering of electrically large and complex target," in *Proc. Int. Appl. Comput. Electromagn. Soc. Symp.-China (ACES)*, Jul. 2018, pp. 1–2.

[5] G. Sundberg, L. M. Zurk, S. Schecklman, and S. Henry, "Modeling rough-surface and granular scattering at terahertz frequencies using the finite-difference time-domain method," *IEEE Trans. Geosci. Remote Sens.*, vol. 48, no. 10, pp. 3709–3719, Oct. 2010.

[6] S.-R. Chai, L.-X. Guo, and R. Wang, "PO–PO method for electromagnetic backscattering from a 2D arbitrary dielectric-coated conducting target located above a 1D randomly rough surface: Horizontal polarisation," *IET Microw., Antennas Propag.*, vol. 8, no. 15, pp. 1340–1347, Dec. 2014.

[7] Z. He, D. Z. Ding, and R. S. Chen, "An efficient marching-on-in-degree solver of surface integral equation for multilayer thin medium-coated conductors," *IEEE Antennas Wireless Propag. Lett.*, vol. 15, pp. 1458–1461, 2016.

[8] P. Usai, M. Borgese, F. Costa, and A. Monorchio, "Hybrid physical optics-MoM-ray tracing method for the RCS calculation of electrically large objects covered with radar absorbing materials," in *Proc. IEEE Int. Symp. Antennas Propag. USNC/URSI Nat. Radio Sci. Meeting*, Jul. 2018, pp. 145–146.

[9] L. Tsang, K.-H. Ding, S. Huang, and X. Xu, "Electromagnetic computation in scattering of electromagnetic waves by random rough surface and dense media in microwave remote sensing of land surfaces," *Proc. IEEE*, vol. 101, no. 2, pp. 255–279, Feb. 2013.

[10] Y. Oh, K. Sarabandi, and F. T. Ulaby, "An empirical model and an inversion technique for radar scattering from bare soil surfaces," *IEEE Trans. Geosci. Remote Sens.*, vol. 30, no. 2, pp. 370–381, Mar. 1992.

[11] N. Pinel, J. T. Johnson, and C. Bourlier, "A geometrical optics model of three dimensional scattering from a rough layer with two rough surfaces," *IEEE Trans. Antennas Propag.*, vol. 58, no. 3, pp. 809–816, Mar. 2010.

[12] X. Duan and M. Moghaddam, "Bistatic vector 3-D scattering from layered rough surfaces using stabilized extended boundary condition method," *IEEE Trans. Geosci. Remote Sens.*, vol. 51, no. 5, pp. 2722–2733, May 2013.

[13] K. Sarabandi and T. Chiu, "Electromagnetic scattering from slightly rough surfaces with inhomogeneous dielectric profiles," *IEEE Trans. Antennas Propag.*, vol. 45, no. 9, pp. 1419–1430, Sep. 1997.

[14] A. Soubret, G. Berginc, and C. Bourrely, "Backscattering enhancement of an electromagnetic wave scattered by two-dimensional rough layers," *J. Opt. Soc. Amer. A, Opt. Image Sci.*, vol. 18, no. 11, pp. 2778–2788, Nov. 2001.

[15] A. Tabatabaeenejad and M. Moghaddam, "Bistatic scattering from three-dimensional layered rough surfaces," *IEEE Trans. Geosci. Remote Sens.*, vol. 44, no. 8, pp. 2102–2114, Aug. 2006.

[16] P. Imperatore, A. Iodice, and D. Riccio, "Volumetric-perturbative reciprocal formulation for scattering from rough multilayers," *IEEE Trans. Antennas Propag.*, vol. 59, no. 3, pp. 877–887, Mar. 2011.

[17] H. Zamani, A. Tavakoli, and M. Dehmollaian, "Scattering from layered rough surfaces: Analytical and numerical investigations," *IEEE Trans. Antennas Propag.*, vol. 54, no. 6, pp. 3685–3696, Jun. 2016.

[18] A. Tabatabaeenejad and M. Moghaddam, "Study of validity region of small perturbation method for two-layer rough surfaces," *IEEE Geosci. Remote Sens. Lett.*, vol. 7, no. 2, pp. 319–323, Apr. 2010.

[19] Z. Li and T. J. Cui, "High frequency methods for simulation of high resolution imaging in terahertz regime," *J. Infr. Millim. Terahertz Waves*, vol. 31, no. 3, pp. 349–357, 2010.

[20] R. Brem and T. F. Eibert, "A shooting and bouncing ray (SBR) modeling framework involving dielectrics and perfect conductors," *IEEE Trans. Antennas Propag.*, vol. 63, no. 8, pp. 3599–3609, Aug. 2015.

[21] R. Wang, C. Zhang, L. X. Guo, and Z. B. Zhang, "Two-layered rough surfaces modeling based on the physical optics in terahertz gap," in *Proc. 6th Asia–Pacific Conf. Antennas Propag. (APCAP)*, Oct. 2017, pp. 1–3.

[22] W. B. Gordon, "Far-field approximations to the Kirchoff–Helmholtz representations of scattered fields," *IEEE Trans. Antennas Propag.*, vol. AP-23, no. 4, pp. 590–592, Jul. 1975.

[23] J. A. Kong, *Electromagnetic Wave Theory*. Hoboken, NJ, USA: Wiley, 1985.

RUI WANG was born in Heyang, China, in 1981. She received the B.S. degree in electronic information science and technology and the Ph.D. degree in radio science from Xidian University, Xi'an, China, in 2004, and 2009, respectively. Her research interests include electromagnetic wave propagation and scattering in complex and random media and computational electromagnetics for remote sensing from target above or below random rough surfaces.

GUANGBIN GUO received the B.S. degree in electronic information science and technology from Xidian University, Xi'an, China, in 2015, where he is currently pursuing the Ph.D. degree in radio science with the Institute of Radio Propagation of the School of Physics and Optoelectronic Engineering. His research interests include applied and computational electromagnetics for remote sensing from target above or below random rough surfaces.

LIXIN GUO (S'95–M'03–SM'16) received the M.S. degree in radio science from Xidian University, Xi'an, China, and the Ph.D. degree in astrometry and celestial mechanics from Chinese Academy of Sciences, China, in 1993 and 1999, respectively. From 2001 to 2002, he was a Visiting Scholar with the School of Electrical Engineering and Computer Science, Kyungpook National University, Daegu, South Korea. He has been a Visiting Professor with the d'Energetique des Systemes et Precedes (LESP), University of Rouen, Mont-Saint-Aignan, France, and Faculty of Engineering and Physical Sciences, The University of Manchester, Manchester, U.K. He is currently a Professor and the Head of the School of Physics and Optoelectronic Engineering, Xidian University, China. He has been a Chief Professor of Innovative Research Team in Shaanxi Province, China, since 2014. He has authored and coauthored four books and over 300 journal papers. He has been in charge of and undertaken more than 30 projects. His research interests include electromagnetic wave propagation and scattering in complex and random media, computational electromagnetics, inverse scattering, antenna analysis and design. He was the recipient of the National Science Fund for Distinguished Young Scholars in 2012, and a Distinguished Professor of Changjiang Scholars Program, in 2014.